DELFT UNIVERSITY OF TECHNOLOGY

AE4-301
AUTOMATIC FLIGHT CONTROL SYSTEM DESIGN

F16 Autopilot System Design

Author:
Yaïr Brouwer 4488989
Godert de Zoeten 4447905

February 23, 2020

List of Symbols

Symbol	Description	Unit
α	Angle of attack	[deg]
β	Sideslip angle	[deg]
γ	Flight path angle	[deg]
δ_a	Aileron deflection	[deg]
δ_{el}	Elevator deflection	[deg]
δ_t	Throttle change	[lb]
δ_r	Rudder deflection	[deg]
θ	Pitch attitude	[deg]
τ	Time constant	[s]
ϕ	Roll angle	[deg]
ψ	Heading angle	[deg]
ζ	Damping ratio	[-]
ω_n	Natural frequency	[rad/s]
a_n	Normal acceleration	[ft/s^2]
p	Roll rate	[rad/s]
P	Period	[s]
q	Pitch rate	[rad/s]
r	Yaw rate	[rad/s]
h	Altitude	[ft]
$\dot{h}$	Descent rate	[ft/s]
h_{flare}	Flare begin altitude	[ft]
K	Feedback gain	varies
M	Mach number	[-]
n	Load factor	[-]
$T_{1/2}$	Time to half-amplitude	[s]
V	Velocity	[ft/s]

1 Introduction

In this report the design of a control system for the Lockheed Martin F16 is described as a part of the 4301-P course practical assignment. The system is designed using classical control theory. First the linearisation and trimming of two different models for the F16 dynamics is described to obtain a state-space representation. Then the influence of the accelerometer position is analysed on the measured normal acceleration. Then an open-loop analysis is performed to determine the period and aperiod eigenmotions of the F16. After that a pitch rate command system is designed and the CAP and Gibson requirements are analysed. The last part of the report consists of the design of an automatic glideslope following and flare controller, followed by concluding remarks.

2 Trimming and Linearising the Low- and High Fidelity F16 Models

In order to be able to evaluate the F16 dynamics, a linear time-invariant system has to be retrieved for both the selected flight condition and the flight condition at which the accelerometer influence is determined. Before the system can be linearised, it has to be trimmed as well. Trimming amounts to minimising a cost function containing the weighted accelerations on the system. The trim point retrieved gives a combination of controls and states that result in the system to be in equilibrium. Trimming before linearising is of importance, as linearising at the trim point gives the most reliable results. This phenomenon can be attributed to the fact that a linearisation loses its significance when a system is changing, hence linearisation is most accurate in steady state.

As the last digit of the student number of the author is a 9 and the author's netID starts with a y, the selected flight condition is at $40\,000\,\mathrm{ft}$ and at a velocity of $900\,\mathrm{ft/s}$. As prescribed by the assignment description, the flight condition for the accelerometer position analysis is taken to be at $15\,000\,\mathrm{ft}$ at a velocity of $500\,\mathrm{ft/s}$.

Two different models are considered: the low-fidelity model [1] and the high-fidelity model [2]. The main differences between these models are that the low-fidelity model does not include the aerodynamic properties of the leading edge slats control surface, while the high-fidelity model does include these. Also, the low-fidelity model completely decouples the longitudinal and lateral equations of motion.

Trimming has been done using the provided *FindF16Dynamics.m* file. The F-16 is trimmed for steady wings-level flight. For both flight conditions the trim point for the high-fidelity model was achieved when the cost function converged to the order of 10^{-6}. For the low-fidelity model the cost function converged to the order of 10^{-29} for both flight conditions. From this it can be seen that the trimming points of the low-fidelity model are closer to a perfectly trimmed point than those of the high-fidelity model. This means that these are also better operating points for linearisation and therefore the LTI systems for the low-fidelity model are more reliable to represent the non-linear system well. Mind, however, that the high-fidelity model could still represent the real-life aircraft better. The results of the trimming process for both flight conditions are shown in Table 2 and Table 3.

Table 2: Linearised model for flight condition with altitude 40,000 ft and velocity 900 ft/s.

Parameter	Low-Fidelity	High-Fidelity
Cost [-]	$2.68 \cdot 10^{-29}$	$1.45 \cdot 10^{-6}$
Thrust [lb]	2107	1914
Elevator [deg]	-2.13	-1.34
Aileron [deg]	$-1.76 \cdot 10^{-15}$	-0.08
Rudder [deg]	$-7.76 \cdot 10^{-15}$	-0.01
α [deg]	3.07	2.88
LE flap [deg]	0	0
Velocity [ft/s]	900	900

Table 3: Linearised model for flight condition with altitude 15,000 ft and velocity 500 ft/s.

Parameter	Low-Fidelity	High-Fidelity
Cost [-]	$2.29 \cdot 10^{-29}$	$7.19 \cdot 10^{-6}$
Thrust [lb]	2121	2109
Elevator [deg]	-2.46	-2.24
Aileron [deg]	$3.21 \cdot 10^{-16}$	-0.09
Rudder [deg]	$2.80 \cdot 10^{-15}$	0.09
α [deg]	4.47	4.53
LE flap [deg]	0	6.28
Velocity [ft/s]	500	500

2.1 Accelerometer Position Influence

In this section the influence on the accelerometer position along the X_b axis on the measured acceleration will be investigated. The conventional body axis system will be used, as shown in Figure 1 [3]. From now on, only the low-fidelity model will be taken into account. Therefore, it will not be specified anymore while talking about the model. In order to investigate the influence that the accelerometer position with respect to the center of gravity has on the functionality of the

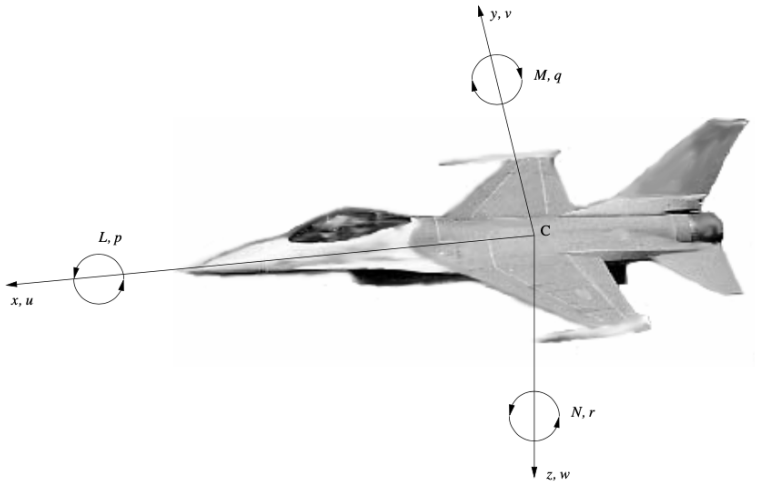

Figure 1: The conventional body axis system as used in this assignment. The accelerometer position will be chosen along the x-axis and measured with respect to the center of gravity position [3]. The positive x-axis points forward through the nose of the aircraft.

accelerometer, the normal acceleration, a_n, has to be included in the outputs of the system, which is done by incorporating the a_n *Definition* block in the F16 simulink model as shown in Figure 2. a_n can be readily retrieved with the available outputs using Equation 1 [4]. Here n_z is the load factor along the z-body axis, $\dot{q}$ is the pitch acceleration, x_a is the accelerometer position with respect to the aircraft center of gravity and g_D is the gravitational acceleration, $g_D = 9.80665$ m/s^2. The content of the aforementioned block can be seen in Figure 3.

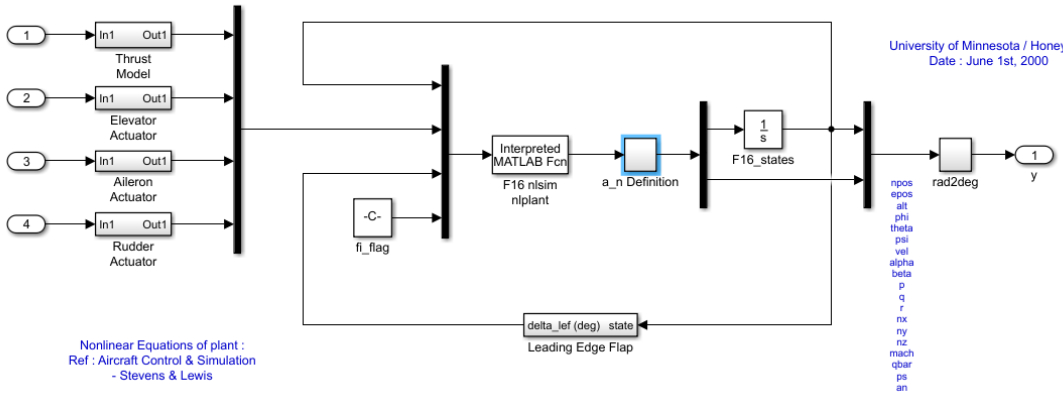

Figure 2: The F16 Simulink model used for the accelerometer influence calculations. In order to acquire the model the definition of the normal acceleration output was incorporated in the model by G.J. Balas [5].

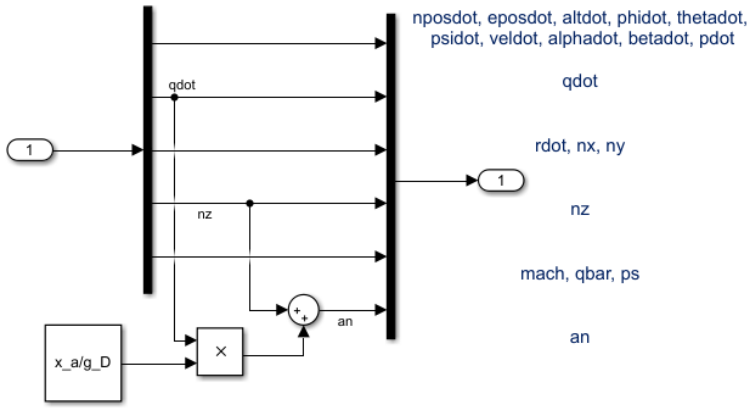

Figure 3: Simulink model used in this assignment.

$$a_n = n_z + \frac{\dot{q}x_a}{g_D} \tag{1}$$

Due to the modification to the simulink model, the output matrix C in the linearised output equation ($y = Cx + Du$) increases from an 18x18 to a 19x18 matrix. Similarly, the feedthrough matrix D increases from an 18x4 to a 19x4 matrix. Isolating a_n, the output equation for the normal acceleration for $x_a = 0$ ft is given by Equation 2. It can be seen that a_n depends on the altitude h, pitch attitude θ, the flight velocity V, the angle-of-attack α, the pitch rate q and the load factor in y-direction n_y. Equation 2 shows that the altitude and pitch attitude have a small influence on the normal acceleration.

$$a_n = \begin{bmatrix} 0 \\ 0 \\ -3.24 \times 10^{-5} \\ 0 \\ -9.68 \times 10^{-6} \\ 0 \\ 0.0040 \\ 9.93 \\ 0 \\ 0 \\ 0.96 \\ 0 \\ 0 \\ 0.021 \\ 0 \\ 0 \\ 0 \\ 0 \end{bmatrix}^T \begin{bmatrix} p_N \\ p_E \\ h \\ \phi \\ \theta \\ \psi \\ V \\ \alpha \\ \beta \\ p \\ q \\ r \\ n_x \\ n_y \\ n_z \\ M \\ \bar{q} \\ p_s \end{bmatrix} + \begin{bmatrix} 0 & 0 & 0 & 0 \end{bmatrix} \begin{bmatrix} T \\ \delta_e \\ \delta_a \\ \delta_r \end{bmatrix} \tag{2}$$

Reducing the B and D matrices to only incorporate the elevator deflection δ_e, the transfer function that relates the normal acceleration to δ_e can be calculated. It is given by Equation 3. The response

of this system to a step input of -10 degrees elevator deflection has been plotted in Figure 4.

$$h(s) = \frac{a_n(s)}{\delta_e(s)} = \frac{0.42s^4 - 1.84s^3 - 22.2s^2 + 0.077s + 0.0012}{s^5 + 21.73s^4 + 33.00s^3 + 41.48s^2 + 0.55s + 0.293} \tag{3}$$

$$= \frac{(s - z_1)(s - z_2)(s - z_3)(s - z_4)}{(s - p_1)(s - p_2)(s - p_3)(s - p_4)(s - p_5)} \tag{4}$$

$$= \frac{(s - 9.76)(s - 0.01)(s + 5.39)(s + 0.006)}{(s + 20.2)(s + 0.76 - 1.21i)(s + 0.76 + 1.21i)(s + 0.004 - 0.08i)(s + 0.004 + 0.08i)} \tag{5}$$

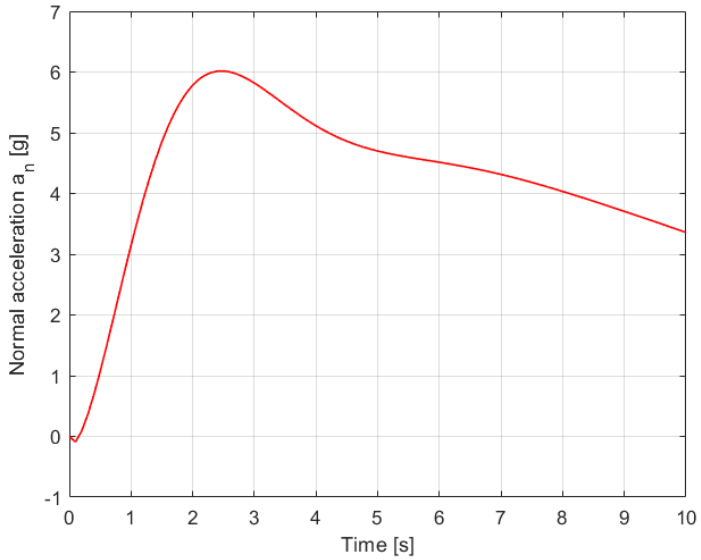

Figure 4: Normal acceleration response of the F-16 to a step input of -10 degrees on the elevator.

It can be seen in Figure 4 that the response moves in opposite direction of the reference signal when it commences (non-miminum phase behaviour). This can be attributed to two zeros of the transfer function in the positive real plane. These zeros are $z_1 = 9.76$ and $z_2 = 0.01$. z_1 contributes most to this non-minimum phase behaviour.

In order to further analyse the effect of the accelerometer position on the normal acceleration response, the position of the zeros and the corresponding responses will be discussed here. Similar systems as the one of Equation 3 have been set up for accelerometer positions of $5\,\text{ft}$, $5.9\,\text{ft}$, $6\,\text{ft}$, $7\,\text{ft}$ and $15\,\text{ft}$. The zeros of these transfer functions for different accelerometer positions are shown in Table 4.

Table 4: Zeros of transfer functions for different accelerometer positions.

Zeros	$x_a = 0$ ft	$x_a = 5$ ft	$x_a = 5.9$ ft	$x_a = 6$ ft	$x_a = 7$ ft	$x_a = 15$ ft
z_1	9.76	40.7	-6.71×10^4	-284	-13.7 + 9.67i	-1.94 + 5.51i
z_2	0.009	0.009	0.009	0.009	0.009	0.009
z_3	-5.39	-8.49	-10.5	-10.9	-13.7 - 9.67i	-1.94 - 5.51i
z_4	-0.006	-0.006	-0.006	-0.006	-0.006	-0.006

When varying the accelerometer position x_a, it can be seen that the non-minimum phase behaviour occurs for all $x_a < 5.9$ ft. It can be seen that for all $x_a < 5.9$ ft the system response first moves down before moving up again, which would be expected in this pull-up manoeuvre. For all of these x_a positions the transfer function has zeros in the right hand plane. For $x_a \geq 5.9$ ft all zeros

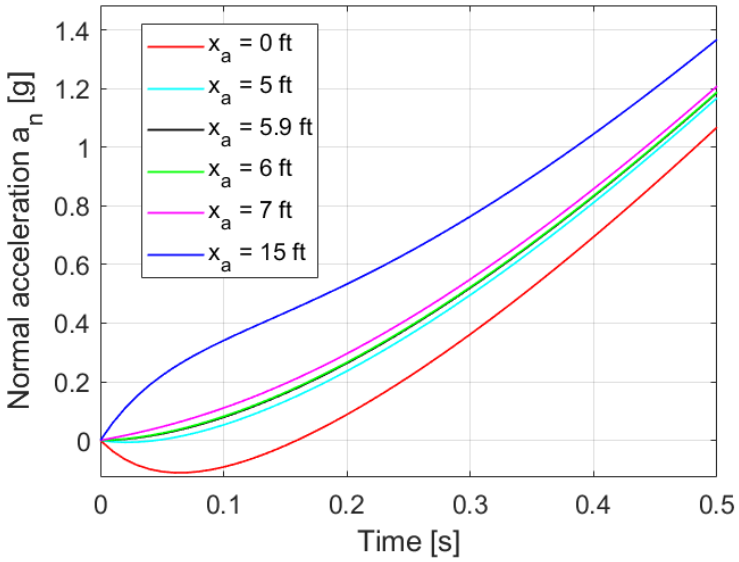

Figure 5: The influence of accelerometer position x_a on the initial response of the accelerometer during a pull-up manoeuvre.

are in the left hand plane except for z_2. However, this zero is so close to the imaginary axis that it has a very small contribution to the non-minimum phase behaviour and it can almost be said that it does not occur: the response moves upward from the start. This can be physically explained by looking at the instantaneous center of rotation.

Apparently the instantaneous center of rotation is located at $x = 5.9$ ft, e.g. at a distance 5.9 ft forward of the center of gravity. When the aircraft performs a pull-up manoeuvre due to an upward deflection of the elevator control surface, the nose of the aircraft rotates upward while the tail rotates downward due to an increase in pitch angle. Therefore, initially all points on the x-axis aft of the instantaneous center of rotation experience a negative normal acceleration before the aircraft as a whole starts to climb. All points on the x-axis forward of the instantaneous center of rotation experience a positive normal acceleration due to the rotation of the aircraft. At the instantaneous center of rotation there is no additional normal acceleration due to rotation. The normal acceleration experienced at that point is entirely due to the aircraft climbing. Figure 5 shows that for $x_a < 5.9$ ft the measured normal acceleration is initially negative, while for $x_a \geq 5.9$ ft the measured normal acceleration is positive from the outset. These effects become stronger when moving further away from the instantaneous center of rotation ($x = 5.9$ ft) because the arm gets larger.

The pilot station should be placed at or in front of the instantaneous center of rotation. The most important thing is that the pilot does not experience non-minimum phase behaviour. Although it is believed that the pilots are extremely well trained, it could still be confusing to initially experience a negative normal acceleration when performing a pull-up manoeuvre. It would be preferrable to either not experience an additional normal acceleration due to aircraft rotation (pilot seat at instantaneous center of rotation), or that the pilot would experience a 'heads up' of the manoeuvre that is about to be performed (pilot station forward of instantaneous center of rotation).

The accelerometer should also be placed close to a node of the most important fuselage bending mode because otherwise the fuselage bending adds additional oscillations to the accelerometer measurements. This will cause inaccuracies in the accelerometer readings, which could cause the SAS to attempt to correct for these oscillations, while they are essentially just noise.

3 Open-Loop Analysis

In this section the inherent flying qualities of the aircraft are evaluated by calculating the motion characteristics of the open loop model. In order to do this, the linearised state space model for the flight condition of 40,000 ft altitude and 900 ft/s velocity is reduced to a 4 states system for both the longitudinal and lateral eigenmotions. For the longitudinal eigenmotions, V_t, α, θ and q are the states of interest. For the lateral eigenmotions, β, ϕ, p and r are the states of interest. In order to reduce the linearised LTI system to the longitudinal and lateral 4 state systems, the original longitudinal and lateral matrices that are shown in Equation 6 to Equation 9 are reduced while actuator dynamics are still included. Then the actuator and engine dynamics are eliminated from the model using the procedure as described below [4]. The model that describes the system from the elevator deflection δ_e to the states can be deduced from the LTI model that describes the system from the actuator input u_{el} and the same states. This principle is shown below. This example is for the longitudinal system. The lateral system can be derived in a similar manner.

$$\dot{x} = \left[\begin{array}{cccc|c} & & A_{a/c} & & B_{a/c} \\ \hline 0 & 0 & 0 & 0 & -a \end{array}\right] \cdot \left[\begin{array}{c} v_T \\ \alpha \\ \theta \\ q \\ \hline \delta_{el} \end{array}\right] + \left[\begin{array}{c} 0 \\ 0 \\ 0 \\ 0 \\ \hline a \end{array}\right] \cdot u_{el}$$

Using this principle, the $A_{a/c}$, $B_{a/c}$, $C_{a/c}$ and $D_{a/c}$ matrices for both longitudinal and lateral systems can be deduced. The original and reduced systems will be presented in the next section.

3.1 Longitudinal and Lateral systems: original and reduced

The original longitudinal system is described by Equation 6 and Equation 7. The lateral systems is represented by Equation 8 and Equation 9.

Original longitudinal system

$$\begin{bmatrix} \dot{h} \\ \dot{\theta} \\ \dot{v_T} \\ \dot{\alpha} \\ \dot{q} \\ \dot{\delta_t} \\ \dot{\delta_e} \end{bmatrix} = \begin{bmatrix} 0.00 & 900 & 7.89 \times 10^{-13} & -900 & 0.00 & 0.00 & 0.00 \\ 0.00 & 0.00 & 0.00 & 0.00 & 1.00 & 0.00 & 0.00 \\ 1.34 \times 10^{-4} & -32.2 & -0.007 & 0.528 & -0.502 & 0.002 & 0.124 \\ 1.44 \times 10^{-6} & -2.07 \times 10^{-13} & -7.90 \times 10^{-5} & -0.466 & 0.975 & -9.346 \times 10^{-8} & -0.001 \\ -2.20 \times 10^{-20} & 0.00 & 1.21 \times 10^{-18} & -2.05 & -0.636 & 0.00 & -0.149 \\ 0.00 & 0.00 & 0.00 & 0.00 & 0.00 & -1.00 & 0.00 \\ 0.00 & 0.00 & 0.00 & 0.00 & 0.00 & 0.00 & -20.2 \end{bmatrix} \begin{bmatrix} h \\ \theta \\ v_T \\ \alpha \\ q \\ \delta_t \\ \delta_e \end{bmatrix}$$

$$+ \begin{bmatrix} 0.00 & 0.00 \\ 0.00 & 0.00 \\ 0.00 & 0.00 \\ 0.00 & 0.00 \\ 0.00 & 0.00 \\ 1.00 & 0.00 \\ 0.00 & 20.2 \end{bmatrix} \begin{bmatrix} u_t \\ u_{el} \end{bmatrix} \tag{6}$$

$$\vec{y} = \begin{bmatrix} h \\ \theta \\ v_T \\ \alpha \\ q \end{bmatrix} = \begin{bmatrix} 1.00 & 0.00 & 0.00 & 0.00 & 0.00 & 0.00 & 0.00 \\ 0.00 & 57.3 & 0.00 & 0.00 & 0.00 & 0.00 & 0.00 \\ 0.00 & 0.00 & 1.00 & 0.00 & 0.00 & 0.00 & 0.00 \\ 0.00 & 0.00 & 0.00 & 57.3 & 0.00 & 0.00 & 0.00 \\ 0.00 & 0.00 & 0.00 & 0.00 & 57.3 & 0.00 & 0.00 \end{bmatrix} \begin{bmatrix} h \\ \theta \\ v_T \\ \alpha \\ q \\ \delta_t \\ \delta_e \end{bmatrix} + \begin{bmatrix} 0 & 0 \\ 0 & 0 \\ 0 & 0 \\ 0 & 0 \\ 0 & 0 \end{bmatrix} \begin{bmatrix} u_t \\ u_{el} \end{bmatrix} \tag{7}$$

Original lateral system

$$\begin{bmatrix} \dot{\phi} \\ \dot{\psi} \\ \dot{v_T} \\ \dot{\beta} \\ \dot{p} \\ \dot{r} \\ \dot{\delta_t} \\ \dot{\delta_a} \\ \dot{\delta_r} \end{bmatrix} = \begin{bmatrix} 0.00 & 0.00 & 0.00 & 0.00 & 1.00 & 0.054 & 0.00 & 0.00 & 0.00 \\ 0.00 & 0.00 & 0.00 & 0.00 & 0.00 & 1.00 & 0.00 & 0.00 & 0.00 \\ 0.00 & 0.00 & -0.007 & -2.77 \times 10^{-15} & 0.00 & 0.00 & 0.002 & 0.00 & 0.00 \\ 0.036 & 0.00 & -3.42 \times 10^{-21} & -0.147 & 0.054 & -1.00 & 0.00 & 1.25 \times 10^{-4} & 3.68 \times 10^{-4} \\ 0.00 & 0.00 & 9.00 \times 10^{-19} & -27.1 & -1.66 & 0.340 & 0.00 & -0.597 & 0.083 \\ 0.00 & 0.00 & 1.19 \times 10^{-18} & 7.80 & -0.018 & -0.228 & 0.00 & -0.034 & -0.061 \\ 0.00 & 0.00 & 0.00 & 0.00 & 0.00 & 0.00 & -1.00 & 0.00 & 0.00 \\ 0.00 & 0.00 & 0.00 & 0.00 & 0.00 & 0.00 & 0.00 & -20.2 & 0.00 \\ 0.00 & 0.00 & 0.00 & 0.00 & 0.00 & 0.00 & 0.00 & 0.00 & -20.2 \end{bmatrix} \begin{bmatrix} \phi \\ \psi \\ v_T \\ \beta \\ p \\ r \\ \delta_t \\ \delta_a \\ \delta_r \end{bmatrix}$$

$$+ \begin{bmatrix} 0.00 & 0.00 & 0.00 \\ 0.00 & 0.00 & 0.00 \\ 0.00 & 0.00 & 0.00 \\ 0.00 & 0.00 & 0.00 \\ 0.00 & 0.00 & 0.00 \\ 0.00 & 0.00 & 0.00 \\ 1.00 & 0.00 & 0.00 \\ 0.00 & 20.2 & 0.00 \\ 0.00 & 0.00 & 20.2 \end{bmatrix} \begin{bmatrix} u_t \\ u_a \\ u_r \end{bmatrix} \tag{8}$$

$$\vec{y} = \begin{bmatrix} \phi \\ \psi \\ v_T \\ \beta \\ p \\ r \end{bmatrix} = \begin{bmatrix} 57.3 & 0.00 & 0.00 & 0.00 & 0.00 & 0.00 & 0.00 & 0.00 & 0.00 \\ 0.00 & 57.3 & 0.00 & 0.00 & 0.00 & 0.00 & 0.00 & 0.00 & 0.00 \\ 0.00 & 0.00 & 1.00 & 0.00 & 0.00 & 0.00 & 0.00 & 0.00 & 0.00 \\ 0.00 & 0.00 & 0.00 & 57.3 & 0.00 & 0.00 & 0.00 & 0.00 & 0.00 \\ 0.00 & 0.00 & 0.00 & 0.00 & 57.3 & 0.00 & 0.00 & 0.00 & 0.00 \\ 0.00 & 0.00 & 0.00 & 0.00 & 0.00 & 57.3 & 0.00 & 0.00 & 0.00 \end{bmatrix} \begin{bmatrix} \phi \\ \psi \\ v_T \\ \beta \\ p \\ r \\ \delta_t \\ \delta_a \\ \delta_r \end{bmatrix} + \begin{bmatrix} 0 & 0 & 0 \\ 0 & 0 & 0 \\ 0 & 0 & 0 \\ 0 & 0 & 0 \\ 0 & 0 & 0 \\ 0 & 0 & 0 \end{bmatrix} \begin{bmatrix} u_t \\ u_a \\ u_r \end{bmatrix} \tag{9}$$

After the reduction procedure previously described was performed, the longitudinal system can be described by Equation 10 and Equation 11. The reduced lateral system is given by Equation 12 and Equation 13.

Reduced longitudinal system

$$\begin{bmatrix} \dot{\theta} \\ \dot{v_T} \\ \dot{\alpha} \\ \dot{q} \end{bmatrix} = \begin{bmatrix} 0.00 & 0.00 & 0.00 & 1.00 \\ -32.2 & -0.007 & 0.528 & -0.502 \\ -2.07 \times 10^{-13} & -7.90 \times 10^{-5} & -0.466 & 0.975 \\ 0.00 & 1.21 \times 10^{-18} & -2.05 & -0.636 \end{bmatrix} \begin{bmatrix} \theta \\ v_T \\ \alpha \\ q \end{bmatrix} + \begin{bmatrix} 0.00 \\ 0.124 \\ -0.001 \\ -0.149 \end{bmatrix} \delta_e \tag{10}$$

$$\vec{y} = \begin{bmatrix} \theta \\ v_T \\ \alpha \\ q \end{bmatrix} = \begin{bmatrix} 57.3 & 0.00 & 0.00 & 0.00 \\ 0.00 & 1.00 & 0.00 & 0.00 \\ 0.00 & 0.00 & 57.3 & 0.00 \\ 0.00 & 0.00 & 0.00 & 57.3 \end{bmatrix} + \begin{bmatrix} 0.00 \\ 0.00 \\ 0.00 \\ 0.00 \end{bmatrix} \delta_e \tag{11}$$

Reduced lateral system

$$\begin{bmatrix} \dot{\phi} \\ \dot{\beta} \\ \dot{p} \\ \dot{r} \end{bmatrix} = \begin{bmatrix} 0.00 & 0.00 & 1.00 & 0.054 \\ 0.036 & -0.147 & 0.054 & -1.00 \\ 0.00 & -27.1 & -1.66 & 0.340 \\ 0.00 & 7.81 & -0.018 & -0.228 \end{bmatrix} \begin{bmatrix} \phi \\ \beta \\ p \\ r \end{bmatrix} + \begin{bmatrix} 0.00 & 0.00 \\ 1.25 \times 10^{-4} & 3.68 \times 10^{-4} \\ -0.597 & 0.083 \\ -0.034 & -0.061 \end{bmatrix} \begin{bmatrix} \delta_a \\ \delta_r \end{bmatrix} \tag{12}$$

$$\vec{y} = \begin{bmatrix} \phi \\ \beta \\ p \\ r \end{bmatrix} = \begin{bmatrix} 57.3 & 0.00 & 0.00 & 0.00 \\ 0.00 & 57.3 & 0.00 & 0.00 \\ 0.00 & 0.00 & 57.3 & 0.00 \\ 0.00 & 0.00 & 0.00 & 57.3 \end{bmatrix} \begin{bmatrix} \phi \\ \beta \\ p \\ r \end{bmatrix} + \begin{bmatrix} 0.00 & 0.00 \\ 0.00 & 0.00 \\ 0.00 & 0.00 \\ 0.00 & 0.00 \end{bmatrix} \begin{bmatrix} \delta_a \\ \delta_r \end{bmatrix} \tag{13}$$

3.2 Inherent motion characteristics

To analyse the inherent behaviour of the aircraft, the periodic and aperiodic eigenmotions are calculated using the reduced longitudinal and lateral systems. The periodic eigenmotions include: short period, phugoid and Dutch roll. The aperiodic eigenmotions include: aperiodic roll and spiral. Also, the time responses of these eigenmotions are plotted.

The natural frequency ω_n, damping ratio ζ and time constant τ are obtained using the Matlab command 'damp'. To determine the eigenmotions, the poles of the reduced longitudinal and lateral systems are used. The longitudinal system has 2 conjugate pole pairs which have an imaginary part. The poles pair closest to the imaginary axis belongs to the phugoid eigenmotion. The poles pair that is further from the imaginary axis belongs to the short period eigenmode. The lateral

system has one complex conjugate poles pair, which belongs to the dutch roll eigenmode. Additionaly, the lateral system also has two purely real poles. The real pole closest to the imaginary axis belongs to the spiral eigenmode, while the real pole further away from the imaginary axis belongs to the aperiodic roll eigenmode.

All periodic eigenmotions are represented by a complex conjugate pole pair. The period of these eigenmotions is calculated using $P = \frac{2\pi}{Im(p)}$, where $Im(p)$ is the imaginary part of the pole. The half-amplitude time is calculated using $T_{1/2} = \frac{ln(1/2)}{Re(p)}$, where $Re(p)$ is the real part of the pole.

3.2.1 Periodic eigenmotions

This section presents the calculated periodic eigenmotions of the aircraft. The natural frequency ω_n, damping ratio ζ, period P and time to half amplitude $T_{1/2}$ are presented in Table 5. The time responses are drawn in Figure 6, Figure 7 and Figure 8.

Table 5: Open-loop dynamics of the F-16 in the periodic eigenmodes, while flying at $900\,\mathrm{ft/s}$ at 40,000 ft.

Eigenmode	ζ **[-]**	ω_n **[rad/s]**	P **[s]**	$T_{1/2}$ **[s]**
Short period	0.364	1.510	4.45	1.26
Phugoid	0.066	0.048	135.16	220.08
Dutch roll	0.07	3.03	2.08	3.12

3.2.2 Aperiodic eigenmotions

This section presents the calculated aperiodic eigenmotions of the aircraft. The time constant τ, natural frequency ω_n and time to half amplitude $T_{1/2}$ are presented in Table 6. The time responses are drawn in Figure 9 and Figure 10.

Table 6: Open-loop dynamics of the F-16 in the aperiodic eigenmodes, while flying at $900\,\mathrm{ft/s}$ at 40,000 ft.

Eigenmode	τ **[-]**	ω_n **[rad/s]**	$T_{1/2}$ **[s]**
Aperiodic roll	0.63	1.559	0.44
Spiral	145.50	0.0069	100.85

3.2.3 Eigenmotion time responses

The time responses of the periodic and aperiodic eigenmotions of the F16 have been plotted in Figure 6-10.

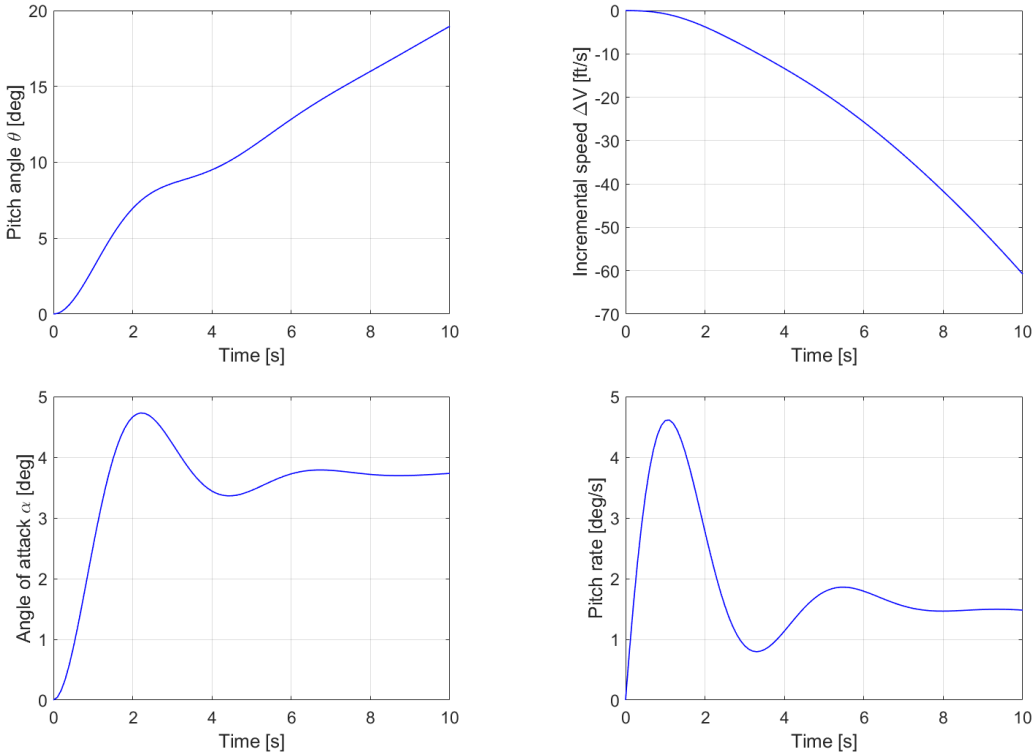

Figure 6: Short period eigenmotion response to a negative elevator deflection step input.

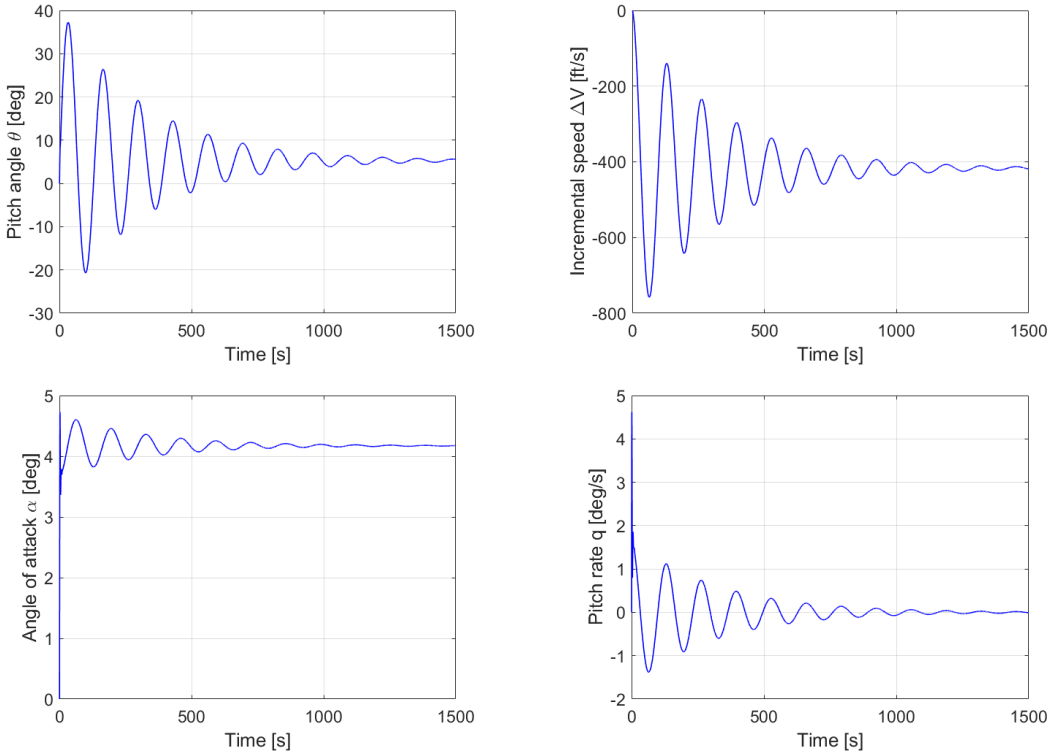

Figure 7: Phugoid eigenmotion response to negative elevator deflection step input.

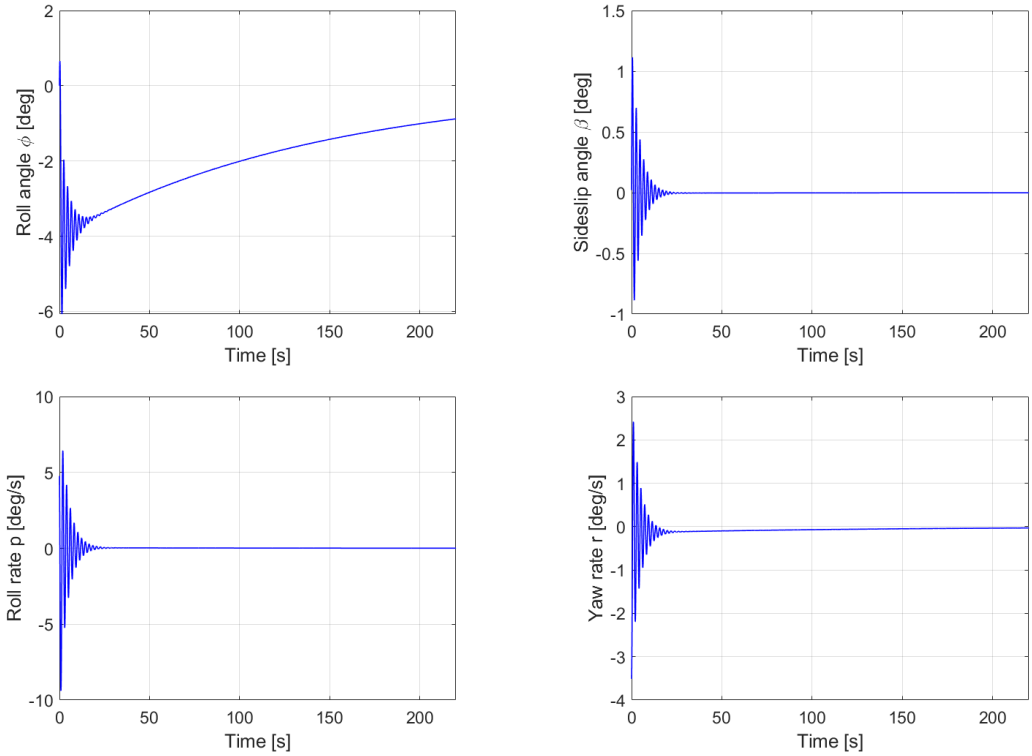

Figure 8: Dutch roll eigenmotion response to a positive rudder deflection impulse input.

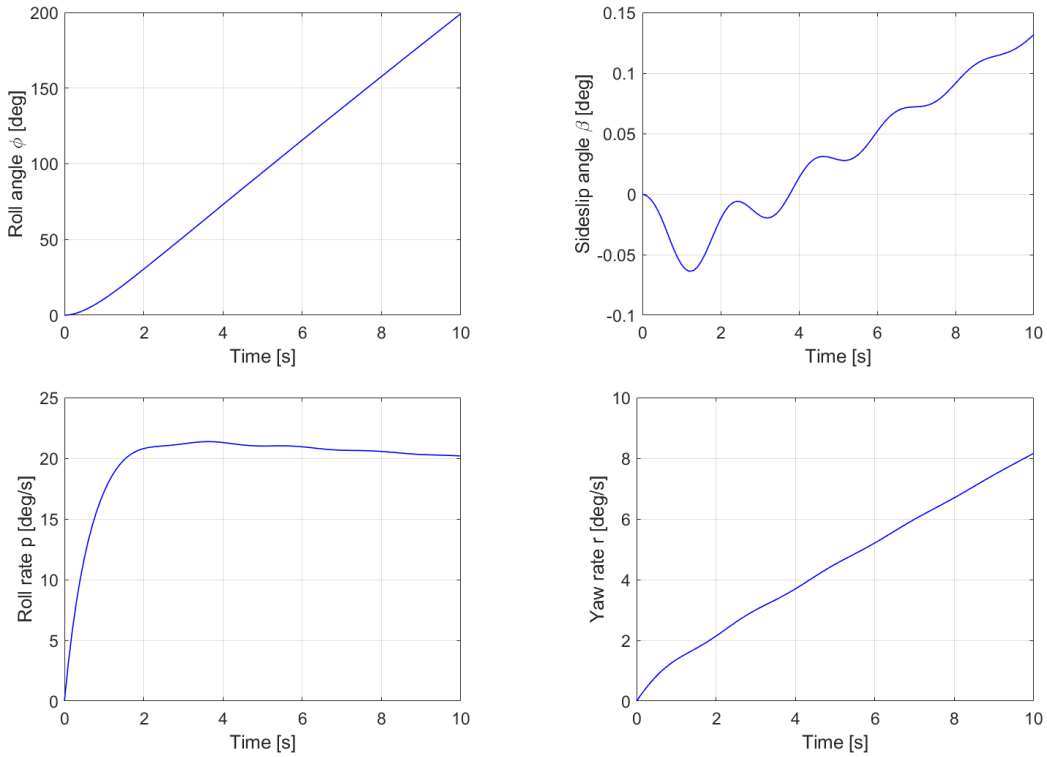

Figure 9: Aperiodic roll eigenmotion response to a negative aileron deflection step input.

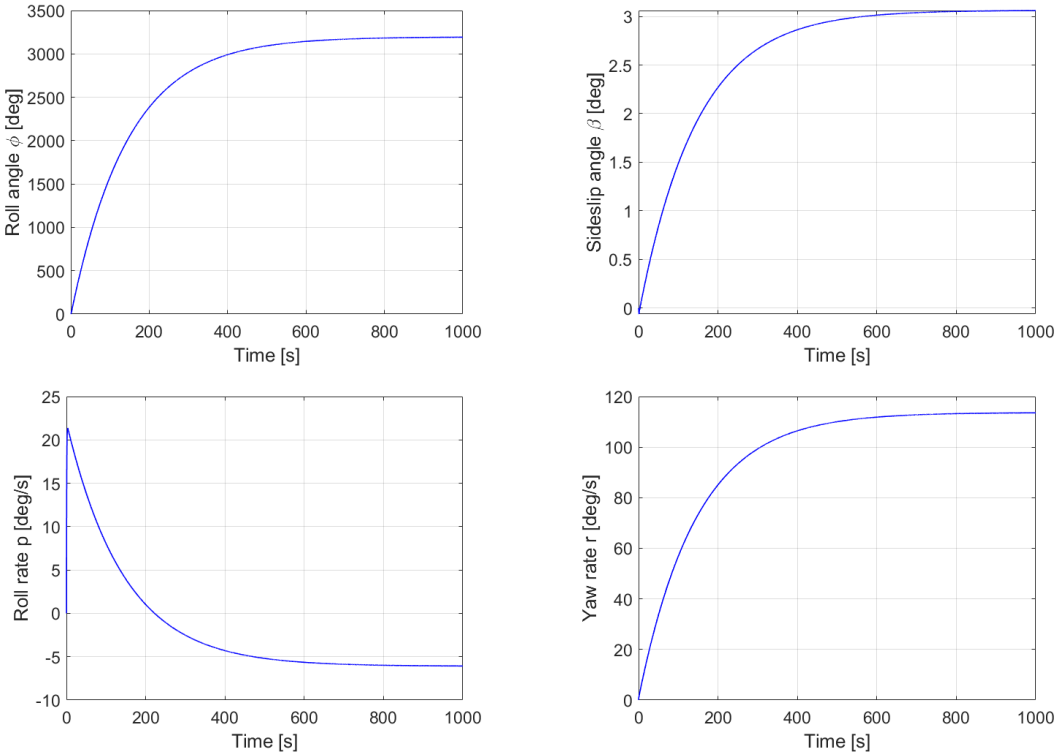

Figure 10: Spiral eigenmotion response to a negative aileron deflection step input.

4 Pitch Rate Command System Design

4.1 Reduction to 2-State System

Before constructing the pitch rate command system, the model for the longitudinal motion without actuator dynamics, which is described by Equation 10 and Equation 11, has to be reduced to a system that describes the short period behaviour using only α and q. This can readily be done by simple reduction, as the actuator dynamics have not been included. The resulting state equation is represented by Equation 14 and the output equation can be seen in Equation 15

$$\begin{bmatrix} \dot{\alpha} \\ \dot{q} \end{bmatrix} = \begin{bmatrix} -0.466 & 0.975 \\ -2.05 & -0.636 \end{bmatrix} \begin{bmatrix} \alpha \\ q \end{bmatrix} + \begin{bmatrix} -9.85 \times 10^{-4} \\ -0.149 \end{bmatrix} \delta_e \tag{14}$$

$$\vec{y} = \begin{bmatrix} \alpha \\ q \end{bmatrix} = \begin{bmatrix} 57.3 & 0.00 \\ 0.00 & 57.3 \end{bmatrix} \begin{bmatrix} \alpha \\ q \end{bmatrix} + \begin{bmatrix} 0.00 \\ 0.00 \end{bmatrix} \delta_e \tag{15}$$

The time responses of the pitch rate q of the 2-state and the 4-state actuator-less systems have been plotted over a short term and over a larger time span in Figure 11. It can be seen that for roughly the first four seconds the responses are almost identical. After the short period motion the oscillatory behaviour of the 2-state system has damped out. For the 4-state system the phugoid poles become dominant, as can be seen in the right-side figure in Figure 11, which shows the long term oscillatory characteristic of the phugoid eigenmotion. The dominant mode is the short period. The 2 state model is valid as in this case only movements in the short term are considered.

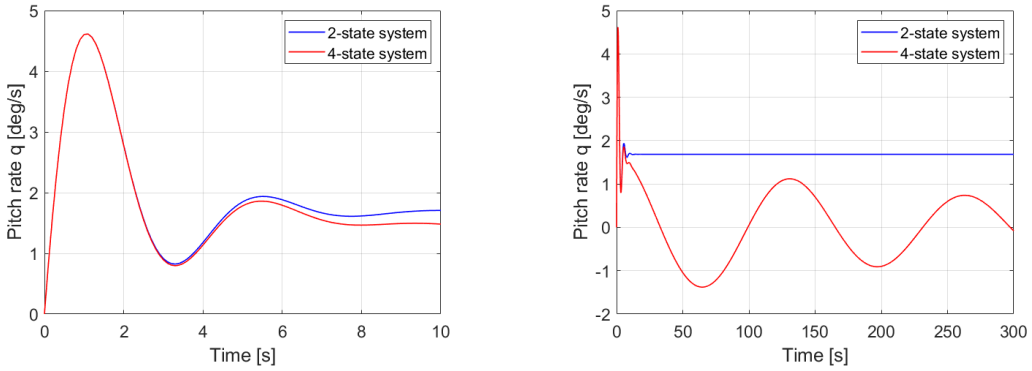

Figure 11: Comparison between the 2 state and 4 state systems without actuator dynamics. The time response to an elevator-up step input is plotted over a short period (left side) and a longer period (right side).

4.2 Pole Placement for Required System Characteristics

The CAP and Gibson criteria impose the following requirements on the system natural frequency ω_n, damping ratio ζ and time constant T_{θ_2}:

- $\omega_{n_{sp}} = 0.03V$, where V is in m/s. This results in a required $\omega_{sp} = 8.2296$ rad/s.
- $T_{\theta_2} = \frac{1}{0.75\omega_{n_{sp}}}$. Required is $T_{\theta_2} = 0.162$ s.
- $\zeta_{sp} = 0.5$.

In order to meet these requirements, the correct feedback gains have to be calculated to place the poles of the system at the required location. The required pole locations are calculated using Equation 16.

$$p_{1,2} = -\zeta_{sp}\omega_{n_{sp}} \pm \omega_{n_{sp}}\sqrt{\zeta_{sp}^2 - 1} \tag{16}$$

This results in the required poles $p_{1,2} = -4.11 \pm 7.13i$. Using the Matlab command 'place', the following feedback gains are calculated:

- $K_\alpha = -426.83$ [deg/rad]
- $K_q = -44.95$ [deg/(rad/s)]

These gains result in the required system characteristics for natural frequency, time constant and damping ratio. The aircraft should be able to handle severe gusts according to MIL-F-8785C, which is a design vertical gust of 4.572 m/s. This gust results in an induced angle of attack of 0.95 degrees according to Equation 17.

$$\alpha_i = \tan^{-1}\left(\frac{V_{gust}}{V}\right) \tag{17}$$

Using the gain value found for K_α the elevator deflection can be calculated with Equation 18. This results in an elevator deflection of -7.11 degrees. This is within the range of acceptable elevator deflection value (-25 to 25 degrees). Therefore the calculated gain is acceptable for handling severe gusts.

$$\delta_{el} = K_\alpha \alpha_i \tag{18}$$

4.3 Lead-Lag Prefilter

In order to modify T_{θ_2} a lead-lag prefilter has to be designed that places the zero at the required location. The lead-lag prefilter will have to be installed outside of the closed loop in order to preserve the pole locations that have been acquired for the $\omega_{n_{sp}}$ and ζ_{sp} requirements.

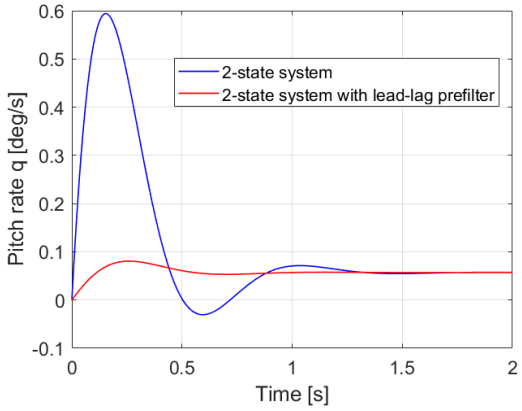

Figure 12: Time response of the filtered and the unfiltered systems.

The closed-loop transfer function with the placed poles is given by Equation 19. It can be seen that this transfer function has a zero at $s = -0.45$. From Equation 20, where T_{θ_2} is equal to 0.162, it can be seen that the required zero should be located at $s = -6.17$. The effect of the lead-lag prefilter on the pitch rate time response can be seen in Figure 12. Clearly, the amplitude of the response has been suppressed significantly by the placement of the zero. However, it can be seen that the stead-state response and the period are the same.

$$\frac{q(s)}{\delta_e(s)} = \frac{-8.551s - 3.866}{s^2 + 8.23s + 67.73} \tag{19}$$

$$\frac{q(s)}{\delta_e(s)} = \frac{k_q(1 + T_{\theta_2}s)}{s^2 + 2\zeta_{sp}\omega_{n_{sp}}s + \omega_{n_{sp}}^2} \tag{20}$$

Using pole-zero cancellation to modify the zero to adhere to the requirement, the lead-lag filter is given by Equation 21. Multiplication with this filter outside of the closed loop results in the transfer function given by Equation 22.

$$f_{LL} = \frac{0.07326s + 0.4522}{s + 0.4522} \tag{21}$$

$$\frac{q(s)}{\delta_e(s)} = \frac{-0.6264s - 3.866}{s^2 + 8.23s + 67.73} \tag{22}$$

4.4 CAP and Gibson criteria

The CAP requirement is calculated using Equation 23[4]. Using the natural frequency, velocity and time constant, it is found that CAP = 0.3922. The CAP value for the given damping ratio is shown in Figure 13 for flight phase categories A, B and C. It can be seen that CAP requirements are satisfied at level 1 for all three flight conditions.

$$CAP = \frac{\omega_{n_{sp}}^2}{\frac{V}{g}\frac{1}{T_{\theta_2}}} \tag{23}$$

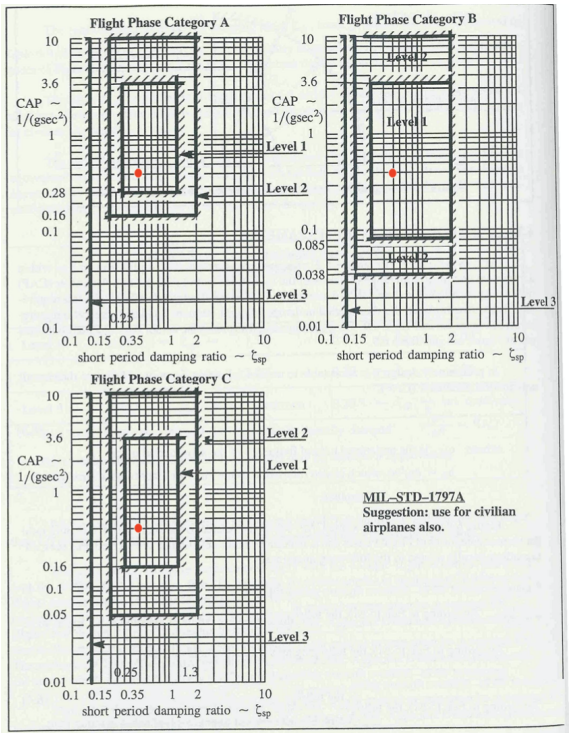

Figure 13: The CAP value (red dot) plotted for flight phases A, B, and C. It can be seen that the CAP value is within level 1 for each flight phase, which is the highest level. Original figure taken from assignment description [4].

For the Gibson requirements, Equation 24 is used [4], as well as $\frac{q_m}{q_s}$, which is the ratio of the maximum pitch rate and the steady state pitch rate.

$$\frac{DB}{q_s} = T_{\theta_2} - \frac{2\zeta_{sp}}{\omega_{n_s p}} \tag{24}$$

In Equation 24, DB is the dropback, the amount of negative transition after the step input has been removed towards the final value. q_s is the steady state pitch rate.
From Equation 24 it can be determined that the design $\frac{DB}{q_s} = 0.0405$. The time responses of the pitch rate and attitude to a step input that is removed at t = 2s are shown in Figure 14. Using these figures, the current point values for $\frac{DB}{q_s}$ and $\frac{q_m}{q_s}$ are calculated which are compared to the design point in Figure 15. From the time responses The current $\frac{q_m}{q_s} = 1.41$ and $\frac{DB}{q_s} = 0.0928$. Figure 15 shows that the system at the current point is within the acceptable Gibson criteria region.

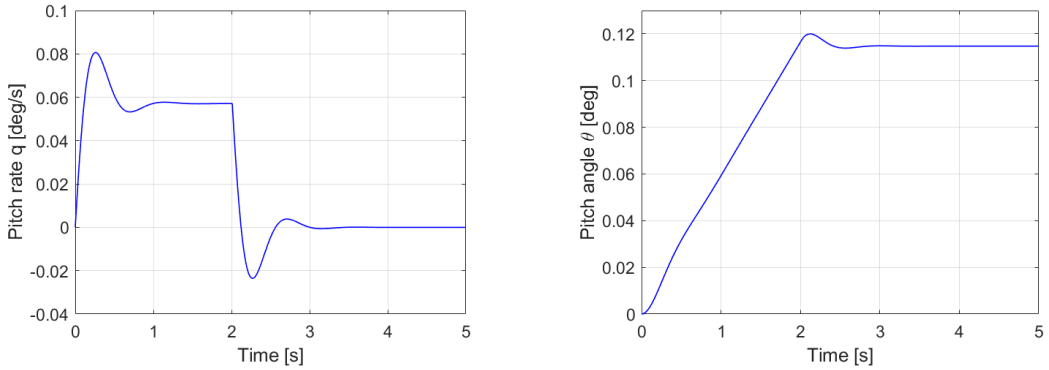

Figure 14: Time responses of the 2-state system with pitch rate command system and lead-lag prefilter, used to calculate $\frac{q_m}{q_s}$ and $\frac{DB}{q_s}$. On the left the pitch rate response to a 2-second negative step input, after which it was returned to 0 degree deflection, has been drawn and on the right the pitch attitude response to the same step has been drawn.

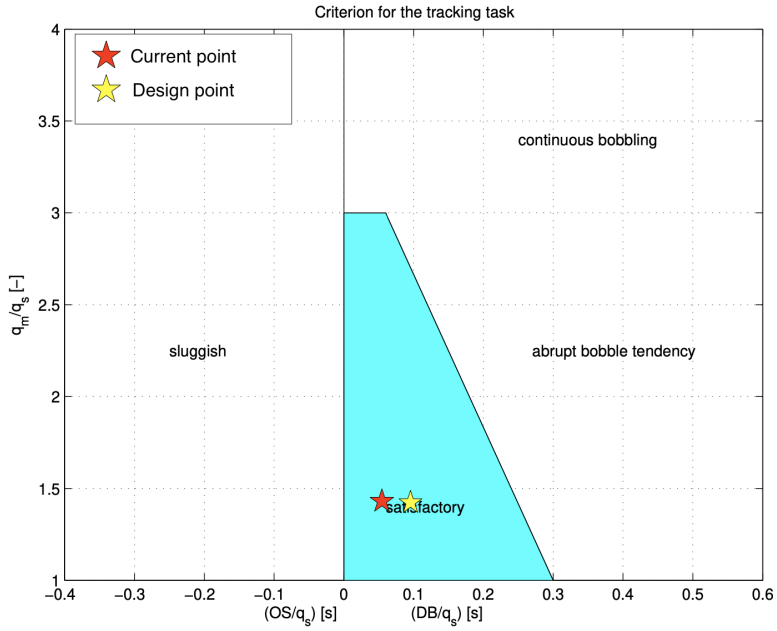

Figure 15: The current and design point of the system plotted in the Gibson criteria map.

5 Design of Automatic Glideslope Following and Flare Controller

This section describes the design of an automatic glideslope following and flare controller. In order to do this the lo-fi model is linearised for a flight condition with velocity 300 ft/s and altitude 5000 ft. Then a reduced model is constructed for five states of interest: the altitude h, the true airspeed v_T, the angle of attack α, pitch attitude angle θ and the pitch rate q.

The reduced systems that are used for the controller design are shown in Equation 25 and Equation 26.

$$\dot{\vec{x}} = \begin{bmatrix} \dot{h} \\ \dot{\theta} \\ \dot{v_T} \\ \dot{\alpha} \\ \dot{q} \end{bmatrix} = \begin{bmatrix} 0 & 300 & 0 & -300 & 0 \\ 0 & 0 & 0 & 0 & 1 \\ 1.32 \cdot 10^{-4} & -32.2 & -0.029 & 2.13 & -2.90 \\ 3.15 \cdot 10^{-6} & 0 & -6.97 \cdot 10^{-4} & -0.54 & 0.915 \\ 0 & 0 & 0 & 0.330 & -0.817 \end{bmatrix} \begin{bmatrix} h \\ \theta \\ v_T \\ \alpha \\ q \end{bmatrix} + \begin{bmatrix} 0 & 0 \\ 0 & 0 \\ 0.0015 & -0.0045 \\ -9.49 \cdot 10^{-7} & -0.0011 \\ 0 & -0.57 \end{bmatrix} \begin{bmatrix} \delta_t \\ \delta_{el} \end{bmatrix} \tag{25}$$

$$\vec{y} = \begin{bmatrix} h \\ \theta \\ v_T \\ \alpha \\ q \end{bmatrix} = \begin{bmatrix} 1 & 0 & 0 & 0 & 0 \\ 0 & 57.3 & 0 & 0 & 0 \\ 0 & 0 & 1 & 0 & 0 \\ 0 & 0 & 0 & 57.3 & 0 \\ 0 & 0 & 0 & 0 & 57.3 \end{bmatrix} \begin{bmatrix} h \\ \theta \\ v_T \\ \alpha \\ q \end{bmatrix} + \begin{bmatrix} 0 & 0 \\ 0 & 0 \\ 0 & 0 \\ 0 & 0 \\ 0 & 0 \end{bmatrix} \begin{bmatrix} \delta_t \\ \delta_{el} \end{bmatrix} \tag{26}$$

The trimmed values of the model parameters are given in Table 7.

Table 7: Linearised model parameters for 300 ft/s velocity and 5,000 ft altitude.

Parameter	Value
Thrust [lb]	2827
Elevator [deg]	-4.19
Velocity [ft/s]	300
Altitude [ft]	5000
Angle of attack [deg]	10.45

The trimmed values in Table 7 should be taken into account when considering the limits of thrust and elevator deflection. The thrust should be between 1,000 lbs and 19,000 lbs and the elevator should not be deflected by more than 25 degrees up or down. The controller accounts for the fact that δ_{el} and δ_t are deviations from the trimmed values, not the total values. The same applies to the airspeed and altitude. To calculate the distance travelled, the approximation position $\approx \frac{v_T}{s}$ is used.

The aircraft is supposed to touch down with a vertical airspeed of between 2 ft/s and 3 ft/s. The airspeed is kept constant at approximately 300 ft/s. Another requirement is that the glidescope of 3 degrees is intercepted 10 seconds into the simulation. The runway is located at an altitude of 3000 ft, so the intercept is at 2000 ft above the ground.

5.1 Control laws

The equations that are used for the two phases of the landing procedure are discussed in this section. The first part consists of following the glideslope. The second part is flaring to prevent the aircraft from touching down with a vertical speed that is too large.

5.1.1 Glideslope control laws

The glideslope is rotated with 3 degrees with respect to the horizon. After 10 seconds into flight the glideslope is intercepted by the aircraft, after which it is supposed to follow this glideslope towards the runway. The situation is sketched in Figure 18.

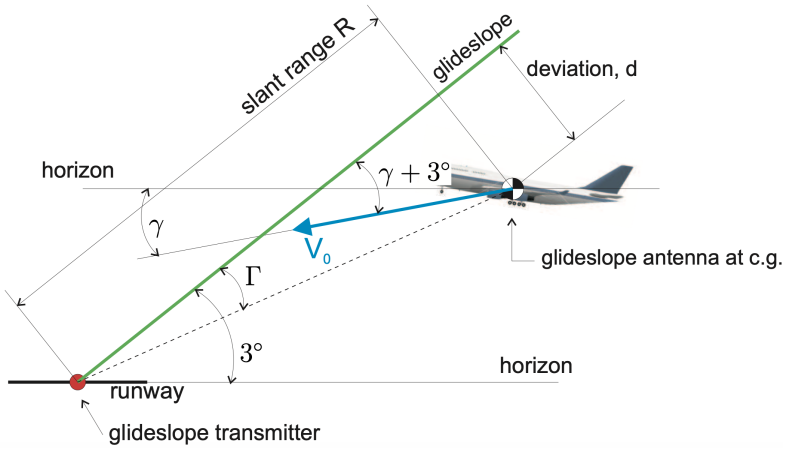

Figure 16: Schematic of glideslope with relevant parameters [6].

The goal of the feedback loop is to reduce the angle Γ to 0 and correct accordingly when the aircraft moves away from the glideslope. This is done with a pitch attitude command system using feedback loops for pitch attitude and pitch rate. To correct accordingly the K_θ block should have a positive gain, and the K_q block should have a negative gain. The values of these gains are presented in the subsection 5.2. The loop feedback gains are tuned from the most inner loop to the most outer loop. The glideslope is governed by the following equations [6]. The small angle approximation has been applied in both cases.

$$d(s) \approx \frac{V_0}{s} \frac{\pi}{180} (\gamma + 3°) \tag{27}$$

$$\Gamma = \text{atan}\left(\frac{d}{R}\right) \approx \frac{d}{R} \tag{28}$$

In Equation 27 γ is the flight path angle, which is obtained from the available system states α and θ through $\gamma = \theta - \alpha$. d is the deviation distance of the aircraft with respect to the glideslope path. In Equation 28 R is the slant range, which is the distance between the aircraft and the glideslope transmitter, as can be seen in Figure 18. Furthermore, a glideslope coupler is used to convert the error in Γ with respect to the reference Γ (which is zero) into a reference pitch attitude. This coupler has the following transfer function:

$$H_{\text{glideslope coupler}} = K_{\text{glideslope}}(1 + \frac{0.1}{s}) \tag{29}$$

The gain $K_{\text{glideslope}}$ also needs to be tuned.

5.1.2 Flare control laws

Towards the end of the glideslope, close to the ground, the flare mode is activated to ensure a smooth but sufficiently firm landing. A schematic of the situation is shown in Figure 17. Note that the value for x_1 as shown in the figure is the chosen design value used in this design. The controller is designed for a vertical speed of 2 to 3 ft/s. This vertical speed is denoted by the descent rate $\dot{h}$.

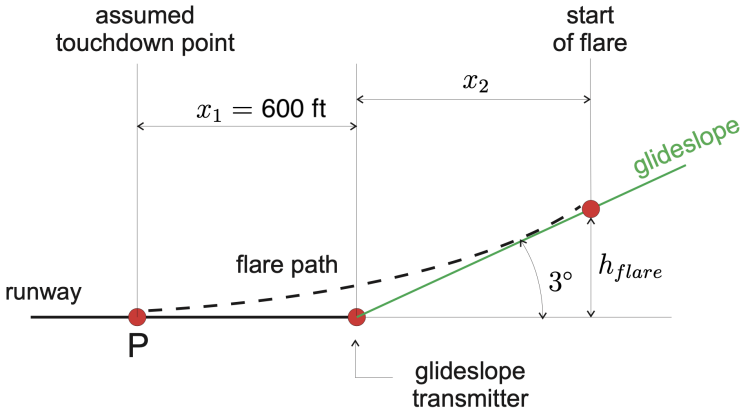

Figure 17: Schematic of flare with relevant parameters [6].

The initial descent rate $\dot{h}_{h_{flare}}$, that is the descent rate at the altitude where the flare is started h_{flare}, is calculated using the glideslope angle and the airspeed using Equation 30.

$$\dot{h}_{h_{flare}} = -\frac{h_{flare}}{\tau} = -V_0 \sin(3°) = -15.7 \text{ft/s} \tag{30}$$

Generally, for the descent rate during flare:

$$\dot{h} = -\frac{h}{\tau} \tag{31}$$

Where τ is the time constant of the flare. It is assumed that the aircraft touches down at $t = 4\tau$, so therefore:

$$x_1 + x_2 = 4V_0\tau \tag{32}$$

Lastly, through the geometry of the situation:

$$x_2 = \frac{h_{flare}}{\tan(3°)} \tag{33}$$

By combining these four equations and choosing the design value for x_1, the design x_2, h_{flare} and τ can be found. These are listed in Table 8.

Table 8: Control gains for the glideslope and flare controller.

Design parameter	**Value**
h_{flare} [ft]	10.46
x_1 [ft]	600
x_2 [ft]	199.6
τ [s]	0.666

5.2 Model Presentation

The block diagram of the controller has been shown below. In order to achieve desirable response characteristics, the gains have been tuned, starting from the inner loops and ending with the glideslope and flare gains. For the inner loops, while tuning K_q, K_θ and K_V a compromise was made between a fast response and oscillatory behaviour. For the glideslope and flare gains, a compromise had to be made between tracking the glideslope and being able to perform the flare manoeuvre in order to decelerate to a rate of descent of $3\,\mathrm{ft/s}$. The resulting gains have been tabulated in Table 9.

Table 9: Control gains for the glideslope and flare controller.

Gain	**Value**
K_q	-10
K_θ	5
K_V	-8000
$K_{\text{glideslope}}$	4000
K_{flare}	0.0855

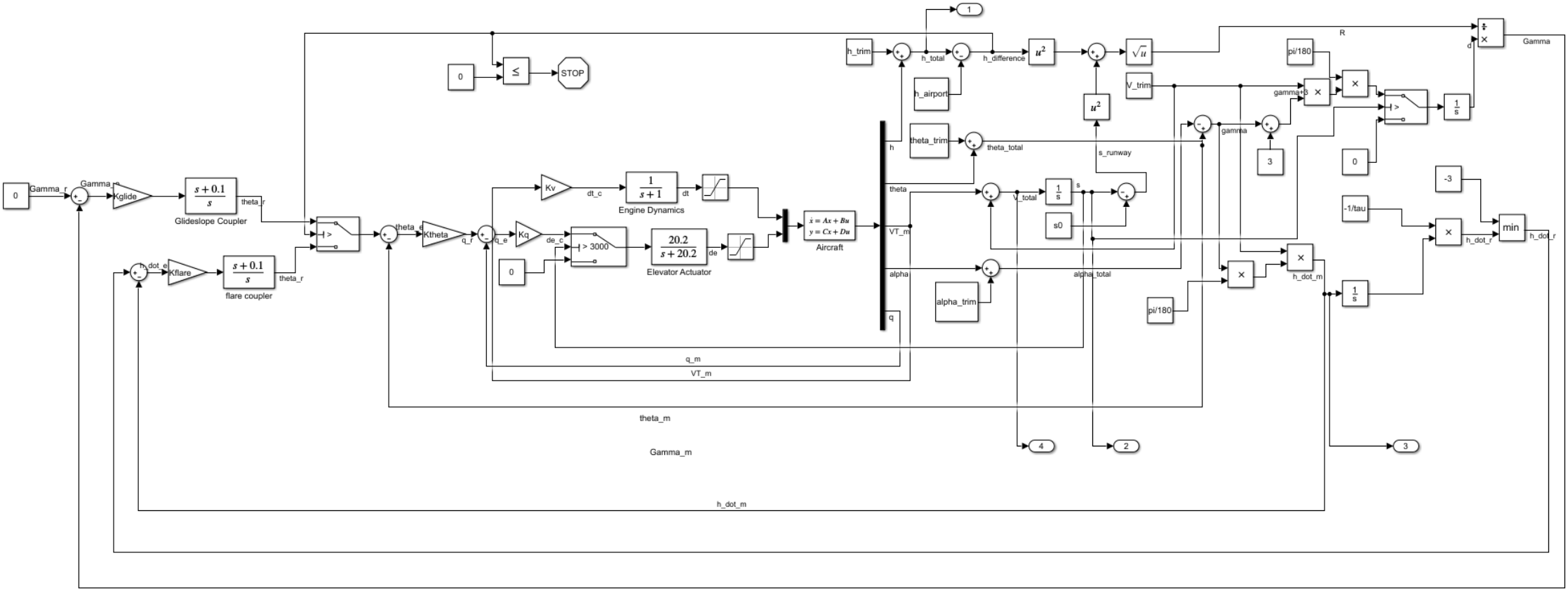
0
Gamma_r
Gamma_e
Kglide
$\frac{s+0.1}{s}$
Glideslope Coupler
theta_r
h_dot_e
Kflare
$\frac{s+0.1}{s}$
flare coupler
theta_r
theta_e
Ktheta
q_r
q_e
Kq
Kv
dt_c
$\frac{1}{s+1}$
Engine Dynamics
dt
de_c
> 3000
$\frac{20.2}{s+20.2}$
Elevator Actuator
de
0
$\dot{x} = Ax + Bu$
$y = Cx + Du$
Aircraft
h
theta
VT_m
alpha
q
0
≤
STOP
1
h_trim
h_total
h_airport
h_difference
u^2
$\sqrt{u}$
V_trim
u^2
theta_trim
theta_total
s_runway
V_total
$\frac{1}{s}$
s
s0
alpha_trim
alpha_total
gamma
3
pi/180
gamma+β
R
d
Gamma
0
$\frac{1}{s}$
-3
-1/tau
min
h_dot_r
h_dot_m
$\frac{1}{s}$
pi/180
q_m
VT_m
theta_m
Gamma_m
h_dot_m
4
2
3

5.3 Simulation Results

Here the results from the simulation with the glideslope following and flare controller are presented. To begin with, the flight path of the F16 over the entire landing manoeuvre has been plotted in Figure 18. It can be seen that the aircraft first flies in level flight at $5000\,\mathrm{ft}$ altitude for approximately $3000\,\mathrm{ft}$, after which it starts the descent. The glideslope angle response takes some time before it tracks the desired glideslope without an error, but after that it tracks it well until the flare manoeuvre is initiated.

The flare manoeuvre has been enlarged in Figure 19. Clearly visible is the deviation from the glideslope angle and the exponential shape of the trajectory that is typical for the flare landing using the aforementioned control laws. The distance x_1 is equal to $177.73\,\mathrm{ft}$, which is shorter than what the controller was been designed for. Also, x_2 is found to be $112\,\mathrm{ft}$, which is shorter than the $199.6\,\mathrm{ft}$ that was designed for.

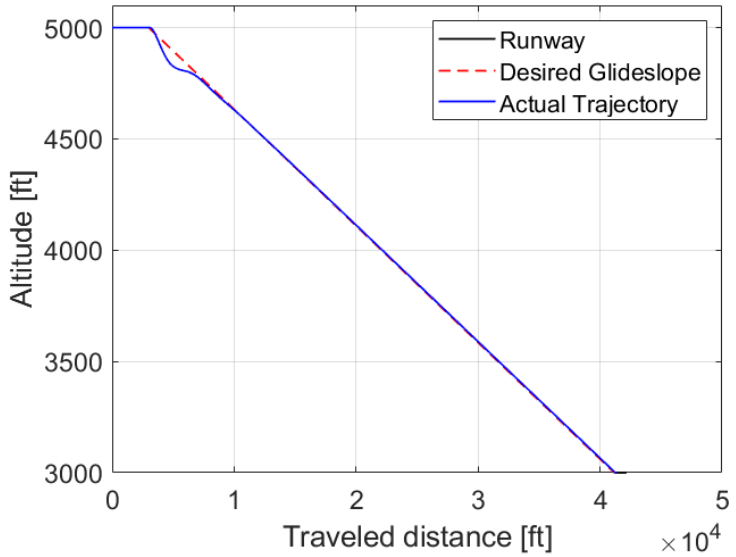

Figure 18: Trajectory of aircraft, compared to the desired glideslope. The aircraft first flies at constant altitude for 10 seconds at $300\,\mathrm{ft/s}$. After it descends to the airfield at $3000\,\mathrm{ft}$ altitude after which it flares and lands.

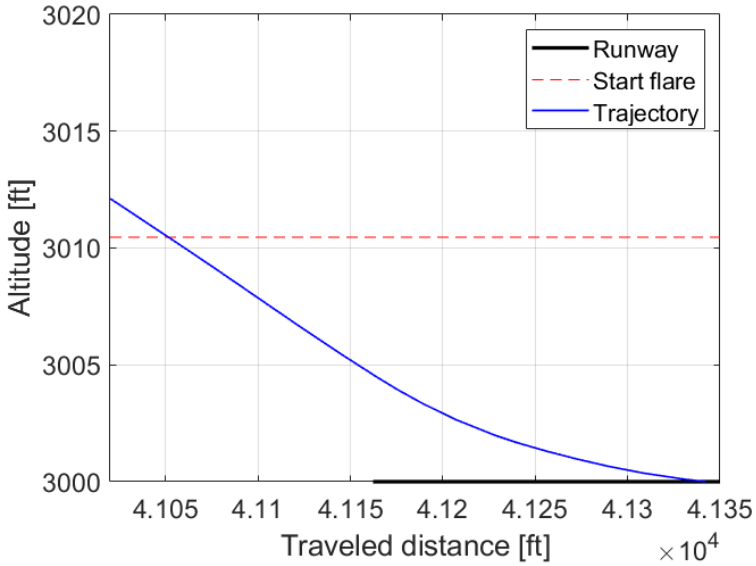

Figure 19: Trajectory of the flare manoeuvre. The flare landing commenced at an altitude of $10.46\,\mathrm{ft}$.

In order to check whether the requirements are still met, even though the distance x_1 does not comply to the design point, the descent rate and the flight speed have been plotted in Figure 20 and Figure 21, respectively. From Figure 20 it can be seen that the rate of descent starts at 0, which is to be expected as it is at level-flight. When the descent starts, the aircraft oscillates around the desired value at first, after which it assumes the expected value of $-V_0 \sin(3°)$. It can be seen that during the flare manoeuvre, the absolute vertical speed is decreased to $-2.46\,\mathrm{ft/s}$, which is within the desirable values. Because of the fact that the aircraft is able to follow the glideslope, the oscillatory behaviour of the descent rate is deemed acceptable.

The flight speed in Figure 21 can be seen to be in the range of $300\,\mathrm{ft}$ over the entire landing procedure. Again, the start of the descent can be distinguished by oscillations in the response. During the flare manoeuvre the aircraft is forced to keep the velocity at a constant $300\,\mathrm{ft/s}$, but it can be seen to decrease to $299\,\mathrm{ft/s}$, which is deemed acceptable. Because of the compromise that had to be made between K_{flare} and K_{glide}, the velocity increment of roughly $8\,\mathrm{ft/s}$ at the start of the descent, which is induced by the oscillatory behaviour, is allowed here.

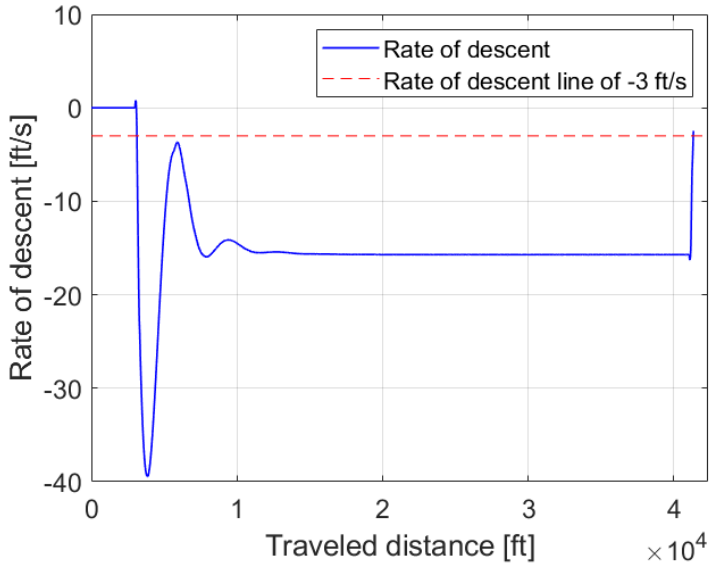

Figure 20: The rate of descent of the aircraft over the entire landing procedure.

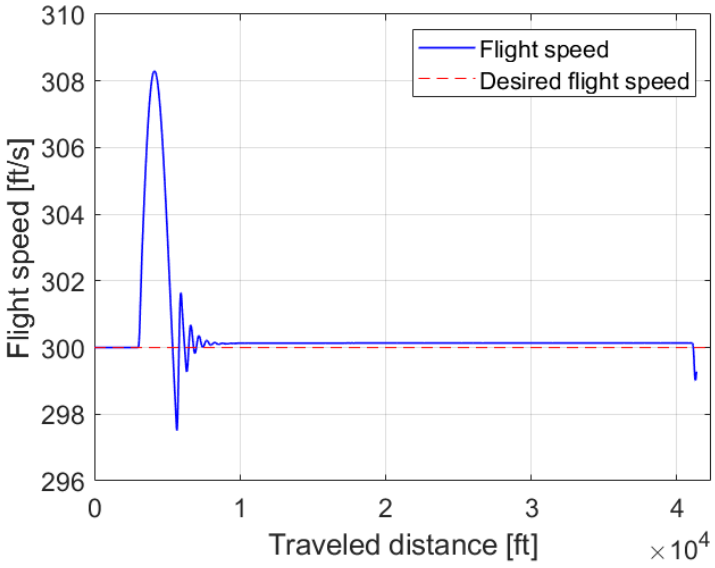

Figure 21: The flight speed of the aircraft over the entire landing procedure.

6 Conclusions

The dynamics of the Lockheed Martin F-16 have been analysed for various flight conditions in this report using the so-called low-fidelity model [1]. This model was linearised and trimmed to find a state space system for the F-16 dynamics. In Chapter 2, the procedure of trimming and linearising has been described and the position of the accelerometer on the normal acceleration measurement has been analysed for a flight condition at 15,000 ft altitude and a velocity of 500 ft/s. It was found that the normal acceleration a_n depended on the altitude, pitch attitude, velocity, angle of attack, pitch rate and load factor in y-direction. It was found that placing the accelerometer behind the instantaneous center of behaviour resulted in non-minumum phase behaviour, which is undesirable. As the instantaneous center of rotation was found to be located at 5.9 ft forward of the center of gravity, it has been advised that the pilot seat should be placed in the instantaneous center of rotation or even further forward.

Chapter 3 conducts an open-loop analysis of the F-16 dynamics at 40,000 ft altitude and 900 ft/s velocity. A reduced longitudinal and lateral system were constructed to analyse the periodic and aperiodic eigenmodes.

In Chapter 4 the reduced longitudinal system from Chapter 3 is reduced even further to only 2 states: angle of attack α and pitch rate . It was found that for short period motions this model performed well compared to a 4 state model as used in Chapter 3. Using a feedback loop and the appropriate feedback gain, the poles of this 2-state system were placed such that the system had the required characteristics for short period natural frequency, time period and damping ratio. The used feedback gain was found to be acceptable when used in the circumstances of a severe gust. To place the zero of the system at the required location, a lead-lag filter was designed which improved the time response considerably. Also, the system characteristics were found to satisfy CAP conditions at level 1 for flight phases A, B, and C. Also the Gibson requirements were met, even though the current point deviated slightly from the design point.

In Chapter 5, an automatic glideslope following and flare controller has been designed to govern the landing procedure. The objective was to eventually touch down at the runway with a vertical velocity of between 2 and 3 ft/s. By tweaking the control gains from the most inner loop to the outermost loop this objective has been attained, with a final descent rate of 2.46 ft/s at touchdown. Also, the aircraft touched down at an acceptable distance from the start of the runway and the glideslope was followed quite well, although it could be improved near the glideslope interception point. The distances x_1 and x_2 are shorter than the values designed for. However, as the aircraft touches down with the correct vertical speed and close to the start of the runway this is deemed acceptable.

References

[1] B.L. Stevens and F.L. Lewis. *Aircraft Control and Simulation*. 2003.

[2] Nguyen and Ogburn. *Simulator Study of Stall / Post-Stall Char- acteristics of a Fighter Airplane with Relaxed Longitudinal Static Stability. Technical Report 1538*. 1979.

[3] R. Russell. *Non-Linear F-16 Simulation using Simulink and Matlab*. 2003.

[4] E. van Kampen. *Practical assignment AE4-301P: Exercise Automatic Flight Control System Design*. 2019.

[5] G.J. Balas. *Non-Linear F16 Model - University of Minnesota*. 2000.

[6] E. van Kampen. *Lecture 14, Automatic Flight Control Design*. 2019.